

**This document was prepared in conjunction with work accomplished under Contract No. DE-AC09-96SR18500 with the U. S. Department of Energy.**

**DISCLAIMER**

**This report was prepared as an account of work sponsored by an agency of the United States Government. Neither the United States Government nor any agency thereof, nor any of their employees, nor any of their contractors, subcontractors or their employees, makes any warranty, express or implied, or assumes any legal liability or responsibility for the accuracy, completeness, or any third party's use or the results of such use of any information, apparatus, product, or process disclosed, or represents that its use would not infringe privately owned rights. Reference herein to any specific commercial product, process, or service by trade name, trademark, manufacturer, or otherwise, does not necessarily constitute or imply its endorsement, recommendation, or favoring by the United States Government or any agency thereof or its contractors or subcontractors. The views and opinions of authors expressed herein do not necessarily state or reflect those of the United States Government or any agency thereof.**

# Tritium Effects on Fracture Toughness of Stainless Steel Weldments

*M. J. Morgan, G. K. Chapman, M. H. Tosten, and S. L. West*  
Westinghouse Savannah River Company  
Savannah River National Laboratory, Aiken, SC, USA

## Abstract

The effects of tritium on the fracture toughness properties of Type 304L and Type 21-6-9 stainless steel weldments were measured. Weldments were tritium-charged-and-aged and then tested in order to measure the effect of the increasing decay helium content on toughness. The results were compared to uncharged and hydrogen-charged samples. For unexposed weldments having 8-12 volume percent retained delta ferrite, fracture toughness was higher than base metal toughness. At higher levels of weld ferrite, the fracture toughness decreased to values below that of the base metal. Hydrogen-charged and tritium-charged weldments had lower toughness values than similarly charged base metals and toughness decreased further with increasing weld ferrite content. The effect of decay helium content was inconclusive because of tritium off-gassing losses during handling, storage and testing. Fracture modes were dominated by the dimpled rupture process in unexposed weldments. In hydrogen and tritium-exposed weldments, the fracture modes depended on the weld ferrite content. At high ferrite contents, hydrogen-induced transgranular fracture of the weld ferrite phase was observed.

## Introduction

Welded stainless steel vessels are used for the containment of tritium gas. Weldments have not been well-characterized with respect to hydrogen and tritium effects (1-8). Weldment properties are different than base metal properties because of the delta ferrite phase which forms during weld solidification. Formation of retained delta ferrite is needed to prevent hot cracking during welding but it could be detrimental with respect to hydrogen and tritium compatibility. The purpose of this work was to characterize the effect of hydrogen isotopes and ferrite content on the fracture toughness properties of weldments. Furthermore, aged tritium-exposed alloys were used to assess the combined embrittlement from tritium and its radioactive decay product, helium-3.

## Experimental Procedure

The compositions of the steels and weld filler materials used in the study are listed in Table I. Type 304L and 21-6-9 stainless steels were used as the base metal and Types 308L, 309L MOD (modified-metal powder cored wire) and 312 MOD were the weld filler wires. The base metal was supplied in one of two forms, forward extruded cylindrical forgings or plates.

For the forging, notched grooves were cut along the length of the forging and the grooves were filled using the gas tungsten arc welding (GTAW) process with one of the filler wires. Figure 1 shows the 304L forging and the welds. A mix of 308L and either 309L MOD or 312 MOD wires were used on the same plate to produce GTAW welds having ferrite contents between 10 and 25%. Electron beam welding was used to produce low ferrite content weldments on the Type 304L plate. A number of weld ferrite morphologies were produced, including a continuous phase. A ferrite scope was used to measure the ferrite content at the root of the notch for each test sample. The weld ferrite contents produced ranged from 4% to 33% by volume. Radiography was used to verify that no unusual porosity, cracking, or other macroscopic defects developed from welding so as to ensure that differences in properties could be attributed to weld microstructure.

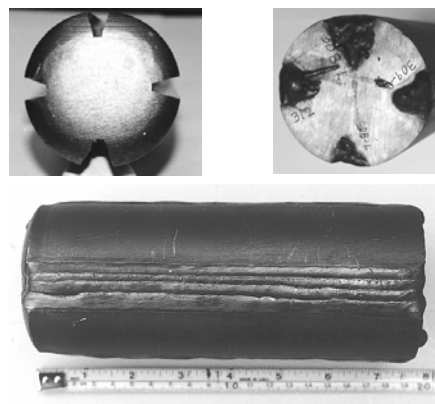


*Figure 1. Type 304L forging with cut grooves and weldments made using Types 308L, 309L MOD, and 312 MOD filler materials.*

Arc-shaped fracture-mechanics specimens having the shape and dimensions shown in Figure 2 were fabricated from the perimeter of each disc and oriented with their notches along the centerline of a weld. The samples were fatigue-cracked so that the crack-length to sample-width ratio was between 0.4 and 0.6.

Four sets of samples were prepared for this study. One set was tested in the as-welded condition. Another set was hydrogen charged at 623 K and a pressure of 35 MPa for three weeks prior to testing. The final two sets were exposed to tritium gas prior to testing. Tritium exposures were identical to the hydrogen exposures. The samples were kept at approximately

223 K prior to testing in order to retain as much of the hydrogen isotopes as possible within the samples after the exposures. One set of tritium-exposed samples was tested soon after charging and 6-month aging, and another tested approximately 24 months later. The temperature of exposure was designed to saturate the samples with hydrogen isotopes without changing their microstructure.

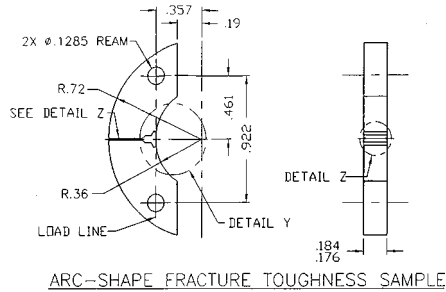


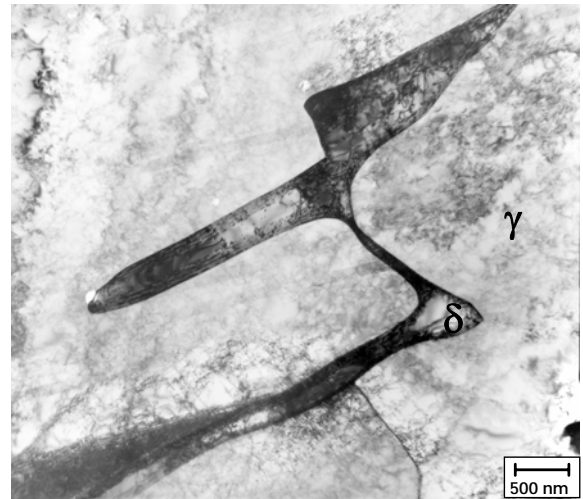
Figure 2. Configuration of fracture toughness sample.

The hydrogen contents of hydrogen-charged samples were measured using a LECO detector. Hydrogen contents were in general agreement with values calculated from hydrogen solubility and diffusivity data for stainless steel and ranged from 125 appm in Type 304L stainless steel to 160 appm for 21-6-9 stainless steel (2). Tritium-charged samples were analyzed for helium concentration from tritium decay at about a mid-point between the two sets of tests on aged samples. Measured helium concentrations in base metals agreed with values calculated from tritium solubility, diffusivity, and decay. Note that the weldments had 33-50% less tritium than base metal because of additional off-gassing losses from weld ferrite. The highest ferrite content weldments had the lowest measured helium contents. Helium contents at the time of each test were calculated from the measured values by accounting for the additional decay of tritium. The results are shown in Table II.

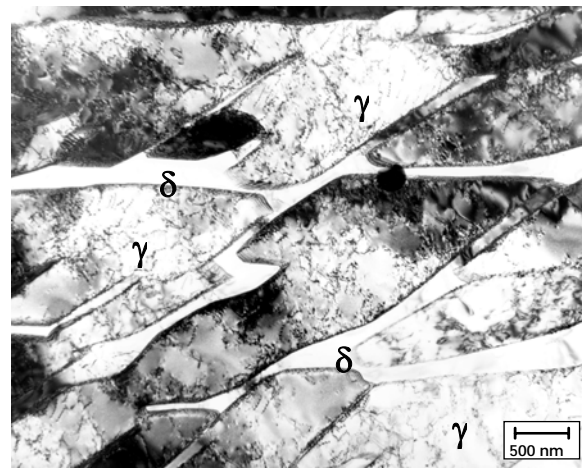
J-integral tests were conducted at room temperature in air using a screw-driven testing machine and a crosshead speed of  $8.5 \times 10^{-4}$  mm / s. while recording load, load-line displacement and crack length. Crack length was monitored using an alternating DC potential drop system and guidelines described in ASTM E647-95 and J-R curves were constructed from the data using ASTM E1820-99 (9).

The weld microstructures were characterized using standard metallographic techniques and transmission electron microscopy. Three to four thin slices were sectioned from each specimen immediately adjacent to the fracture surface and within the weld zone (when present) providing samples with a range of microstructures and deformation levels. Two, 3 mm diameter disks were punched from each slice. Thin foils were prepared from these disks in a Fischione jet-polishing apparatus using a 57% methanol, 39% butylcellosolve, and

4% perchloric acid solution at 35 V DC and 243K. All microscopy was performed using a JEOL 2010 operating at 200 kV.



(a)



(b)

Figure 3. (a) Low Ferrite Weld From 308L Filler Wire and 304L Base Metal and (b) High Ferrite Weld From 312L MOD Filler Wire and 304L Base Metal.

## Results

### Microstructural Characterization

Type 304L austenitic stainless steel consisted of a duplex structure of retained delta ferrite in austenite. Figure 3 shows that welds with ferrite contents less than 8% had microstructures consisting of discontinuous skeletal ferrite present in a predominant austenite matrix and that welds with ferrite content more than 20% had microstructures consisting of nearly continuous ferrite present in a plate-like (or lathy) morphology and globular austenite matrix. These microstructures represent the extremes of the ferrite contents

in the study. The weld microstructures contained a dispersion of fine inclusions produced during welding. The size and spacing of these inclusions can have a significant impact on fracture and fracture toughness.

Tritium-charged samples were also examined using TEM. Figure 4 shows typical helium bubble defects that are observed within the austenite phase of the welds. Helium bubbles, visible in the recrystallized grains and measuring 1-2 nm in diameter, were randomly distributed throughout the grain interiors. In contrast, in regions with a high dislocation density very few bubbles were observed.

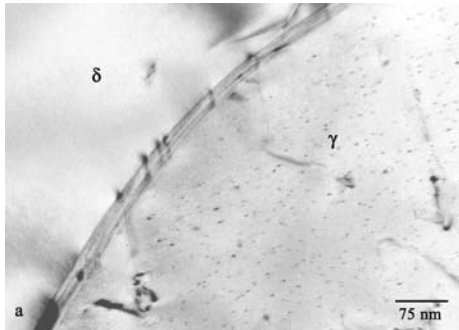


Figure 4. TEM image of an austenite/ferrite interface and the helium bubble distribution in the austenite grain in. The small, black “dots” in the austenite arise from strain contrast associated with helium bubbles.

The helium bubble distribution illustrated in Figure 4 was typical of all welds examined, irrespective of ferrite content. This particular region is from a weld containing the normal level of ferrite in a 304L/308L weld. Helium bubbles were observed only in the austenite matrix and not in the ferrite, on dislocations, or at austenite/ferrite or austenite/austenite boundaries. The failure to observe bubbles at these other locations does not necessarily preclude their presence, since bubbles measuring approximately <math>0.8\text{ nm}</math> are difficult to discern above the background image contrast. Additionally, the magnetic nature of ferrite in welded samples makes focusing TEM images at high magnifications difficult to perform.

For base metal microstructures, helium bubbles were visible in patches of recrystallized grains but not in the cold-worked grains. This is most likely an artifact of the technique because the strain contrast needed for bubble observation is obscured by the strain contrast of the dislocations.

### Fracture Toughness Tests

The J-integral fracture toughness data were collected and calculated from the load-displacement records and the crack length measurements. Typical J-da plots for the steels are shown in Figures 5. The data show that the unexposed weldments containing low ferrite content had fracture toughness values two-to-three times higher than the base

metal. When ferrite morphology is discontinuous (<math>< 12\%</math>) it improves resistance to crack propagation. Note the steep slope for the J-da 308L weld data of Figure 5.

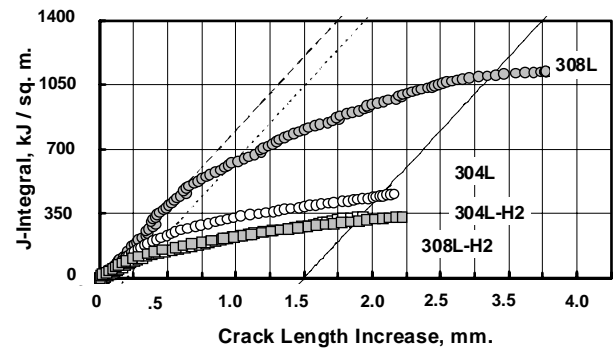


Figure 5. Effect of Hydrogen on J-da Behavior for Type 304L and Type 304L/308L Weldment.

The 308L weld had the highest toughness and the steepest J-R curve indicating its large resistance to crack extension. As the ferrite content increased to 24%, the toughness dropped and the J-R curve flattened out. The 309L MOD weld had the lowest toughness and a shallow sloped J-R curve (33% ferrite).

For hydrogen-exposed welds, ferrite had a detrimental effect on fracture toughness. The fracture path in hydrogen exposed samples changed from dimpled rupture in low-ferrite (<math>< 4\%</math>) welds to fracture along the austenite-ferrite interfaces in medium- ferrite (~12 %) welds to fracture through the ferrite phase in high-ferrite (20-30 %) welds. The hydrogen-charged weldments had fracture toughness values ranging from 388 kJ / sq. m. for welds having normal ferrite contents to less than 30 kJ / sq. m. in welds having high ferrite contents (Figure 6).

Tritium-exposed samples were tested in two groups at different times to measure any toughness decrease caused by the build-in of helium from tritium decay. The first set of aged tritium-exposed weldments showed a reduction in toughness that was consistent with the reduction seen in the hydrogen-charged alloys. This was expected because the helium concentration from tritium decay was low.

The second set of tritium-exposed weldments was tested after a 24 month age. While the base metals showed a reduction in toughness with the increased aging, the weldments did not (Figure 7). One explanation for the discrepancy between the aging effects in weldments and base metals is that weld ferrite leads to tritium off-gassing losses during exposures and storage. This is discussed further below.

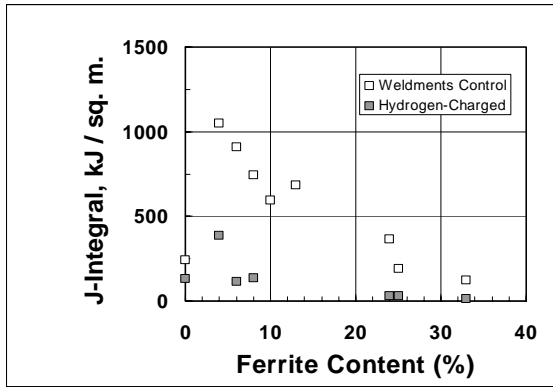


Figure 6. Effects of Hydrogen and Ferrite Content on Fracture Toughness of Type 304L Stainless Steel and its Weldments.

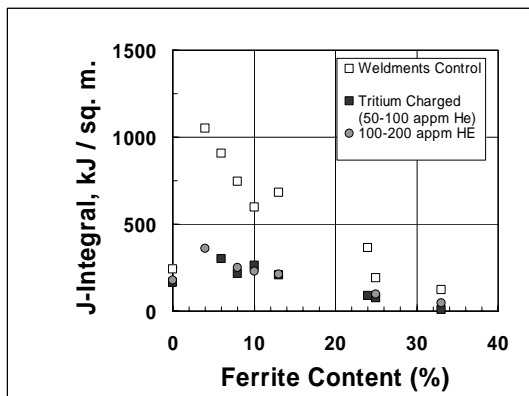


Figure 7. Fracture Toughness of Tritium Exposed Weldments Were Lower than Unexposed Steels at all Ferrite Levels. Aging Time Did Not Reduce Toughness.

### Fractography

Fracture surfaces were examined using scanning electron microscopy. In unexposed specimens, failure was dominated by the growth and coalescence of voids that had nucleated at inclusions. Weldment fracture surfaces were characterized by finer voids than those on base metal fracture surfaces. The fracture path in hydrogen exposed samples changed from dimpled rupture in low-ferrite (< 4%) welds to fracture along the austenite-ferrite interfaces in medium-ferrite (< 12 %) welds to fracture through the ferrite phase in high-ferrite (20-30 %) welds. The fracture mode did not change significantly with aging time for the weldments.

### Discussion

Weldments having normal weld ferrite contents (8-12%) had higher fracture toughness values than the base metals. The toughness of weldments increased with ferrite content at low-to-normal weld ferrite contents but decreased at high levels.

At low ferrite concentrations the toughness improvement that resulted from weld ferrite is in agreement with the stainless steel weldment behavior described in a recent review by Mills (5). Mills indicates that ferrite phases in austenitic stainless steel weldments are brittle at low temperature and stainless steel welds exhibit a ductile-brittle transition temperature phenomenon. However, at ambient and elevated temperatures, Mills shows that the ferrite phase behaves in a ductile manner, and welds are more resistant to fracture. Weldments in this study failed by a similar fracture process that Mills describes with microvoids nucleating at precipitates like manganese silicates and silicides, oxides, and delta-ferrite particles.

The decrease in fracture toughness with weld ferrite content results from two factors. The first factor that contributes to reduced toughness is that the weld yield strength increased with weld ferrite content (Table III). Fracture toughness generally decreases with increasing yield strength. Another contributing factor to the reduced toughness at higher ferrite contents, however, is that the filler wires used to make the high ferrite content welds had a higher concentration of microscopic precipitates than the base metals and the low ferrite fillers. This was seen qualitatively in the metallographic sections and transmission electron micrographs. Higher numbers of precipitates would result in more potential microvoid nucleation sites and less strain needed to link up adjacent voids during the fracture process. The smaller voids were seen on the fracture surfaces and the lower strains to fracture result in lower fracture toughness.

With regard to the effects of hydrogen on the weldment toughness, the fracture modes of the hydrogen-exposed alloys are similar to observations on the effects of hydrogen made by other researchers (1,6). Brooks suggests that fracture occurs along or near the austenite-ferrite boundary in those welds that exhibit hydrogen induced fracture mode changes (1). Luppó also investigated the effects of delta ferrite on hydrogen embrittlement of austenitic stainless steel welds (6). A hydrogen-microprint technique was used to demonstrate that ferrite austenite interfaces acted as traps for hydrogen. This is consistent with the fracture paths observed in the hydrogen and tritium exposed weldments seen in this study particularly at the high ferrite levels. Luppó also observed that ferrite increased the susceptibility to hydrogen embrittlement as measured by ductility losses in tensile tests. In those tests, fracture occurred by cleavage in the ferrite and in the ferrite-austenite interfaces with some tearing in the austenite. This is very similar to fracture mode changes observed here. In low ferrite weldments the ferrite morphology was discontinuous; in high ferrite welds the morphology was continuous (Figure 3). When weld ferrite morphology was discontinuous, fracture toughness values were higher than the base metal; when the ferrite morphology was continuous, fracture toughness values were lower than the base metal.

While the base metals showed a reduction in toughness with the increased aging, the weldments did not. The most likely

explanation for the discrepancy between the aging effects in weldments and base metals is that weld ferrite leads to tritium off-gassing losses during exposure and storage. Note that Table II shows that measured helium concentrations of weldments are lower than base metal concentrations for these tritium exposures. Toughness would not decrease as much with aging time if much of the tritium had already decayed or losses were significant due to off-gassing. Estimated concentrations of helium in the base metal were in agreement with measured values while weldment values were not. Weldments also showed significant tritium off-gassing during the cracking process which indicates that tritium is being lost during the test as well.

Tritium-exposed-and-aged weldments fracture in ways that are similar to those described by researchers who have investigated fracture of irradiated stainless steels. For example, O'Donnell demonstrated that irradiation of 4 dpa of weld metal of 316 severely lowered the J-R curve (7). In this study, both hydrogen and tritium-exposed steels had lower J-R curves than unexposed steels (e.g. Figure 5). In this and O'Donnell's study welds were more significantly affected than the wrought metal (Figure 7). A significant microstructural feature in the weld metal of these studies is the dispersion of fine inclusions produced during welding. The combination of higher particle volume fraction and continuous weld ferrite had their most severe effects on toughness when hydrogen and tritium were present.

## Conclusions

1. Fracture toughness values of stainless steel weldments were higher than the base metal values for weldments with normal weld ferrite contents. Fracture toughness decreased to about half the base metal value as ferrite content was increased from 8% to 33%.

2. Weld microstructure affected fracture toughness. When weld ferrite morphology was discontinuous, fracture toughness values were higher than base metal values; when the ferrite morphology was continuous, fracture toughness values were lower than base metal values.

3. Hydrogen-charged weldments had lower toughness than hydrogen-charged base metals and the toughness decreased with increasing weld ferrite content. Similarly, tritium-exposed-and-aged base metals and weldments had lower toughness than unexposed alloys. The effects of hydrogen and tritium were greatest in the high ferrite welds and were manifested by a change in fracture mode.

4. Base metal toughness decreased with aging time because of increased helium content from tritium decay. Weldment toughness did not decrease with aging time because of tritium off-gassing.

5. Fracture modes were dominated by the dimpled rupture process in unexposed steels and welds. In hydrogen and tritium-exposed welds, the fracture modes depended on the weld ferrite content. At high ferrite contents, fracture occurred predominantly by transgranular cleavage through the weld ferrite phase.

## References

1. Brooks and A. J. West, *Hydrogen Induced Ductility Losses in Austenitic Stainless Steel Welds*, *Metallurgical Transactions A*, 12A, 213-223 (1981)

2. G. R. Caskey, Jr., *Hydrogen Effects in Stainless Steels, Hydrogen Degradation of Ferrous Alloys*, p. 822, ed. J. P. Hirth, R. W. Oriani, and M. Smialowski, eds., Park Ridge, NJ: Noyes Publication, (1985)

3. *Proc. Fourth Int. Conf. on Hydrogen Effects on Material Behavior*, ed. A. W. Thompson and N. R. Moody, Warrendale, PA: The Minerals, Metals & Materials Society, (1989)

4. M. J. Morgan and M. H. Tosten, *Tritium and Decay Helium Effects on the Fracture Toughness Properties of Types 316L, 304L, and 21Cr-6Ni-9Mn Stainless Steels*, p. 873, *Hydrogen Effects in Materials*, ed. A. W. Thompson and N. R. Moody, Warrendale, PA: TMS, (1996)

5. W. J. Mills, *Fracture Toughness of Type 304 and 316 Stainless Steels and Their Welds*, *International Materials Reviews*, 42 (2), 45-82 (1997)

6. M. I. Lупpo, A. Hazarabedian, and J. Ovejero-Garcia, *Effects of Delta Ferrite on Hydrogen Embrittlement of Austenitic Stainless Steel Welds*, *Corrosion Science*, 41, 87-103 (1999)

7. J. O'Donnell, H. Huthmann, and A. A. Tavassoli, *The Fracture Toughness Behavior of Austenitic Steels and Weld Metal Including the Effects of Thermal Aging and Irradiation*, *Int. J. Pres. Ves. & Piping*, 65, 209-220 (1996)

8. S. L. Robinson, *The Effects of Tritium on The Flow and Fracture of Austenitic Stainless Steels*, p. 433, *Proc. Fourth Int. Conf. on Hydrogen Effects on Material Behavior*, ed. A. W. Thompson and N. R. Moody, Warrendale, PA: The Minerals, Metals & Materials Society, (1989)

9. ASTM E 647-95a *Standard Test Method for Measurement of Fatigue Crack Growth Rates* and E 1820-99 *Standard Test Method for Measurement of Fracture Toughness*, ASTM Annual Book of ASTM Standard Volume 3.01 *Metals-Mechanical Testing; Elevated and Low-Temperature Tests; Metallography*, American Society for Testing and Materials, (1999)

**Table I.** Compositions of Stainless Steel Forgings, Plates and Weld Filler Wires (Weight %)

Element	Form	Cr	Ni	Mn	Mo	C	Si	Cu	P	S	N	Co	O	Al
304L*	Forging (Base)	18.0	11.3	1.7	0.04	0.02	0.42	-	0.01	0	0.04	0.03	-	--
304L*	Forging (Weldment)	19.9	10.4	1.7	0.04	0.03	0.63	-	0.02	0	0.04	0.03	-	-
304L	Plate*	17.8	11.1	1.9	0.2	-	0.54	0.12	0.06	-	-	0.07	-	-
21-6-9	Forging	19.3	6.7	9.9	-	0.03	0.38	-	0.01	0	0.28	-	0	0
308L	Filler	20.5	10.3	1.56	<0.01	0.03	0.5	0.02	0.01	0.01	0.06	0.07	-	-
309LM	Filler	23.5	8.55	1.2	2.5	0.02	0.64	0.31	0.02	0.01	-	-	-	-
312 M	Filler	28.7	9.17	1.45	0.27	0.05	0.51	0.31	0.02	0.01	-	-	-	-

\*304L composition from SRS ICPES analysis; all other heats are manufacturers' supplied compositions.

**Table II.** Tritium and Helium Contents for Tritium-Exposed-And-Aged Weldments

Material Description	Original Tritium Content (Calculated) appm	Helium Content (measured) appm	Calc. Helium Content (1st Aging Tests) appm	Calc. Helium at (2 <sup>nd</sup> Aging Tests) appm
Type 304L	1607	129.0	60	198
Type 21-6-9	2005	161.0	75	250
HERF 21-6-9	2641	212.0	98	329
304L EB Weld	1276	86.0	30	143
304L/308L/312L	1251	84.3	30	141
304L/308L/309LM	1316	88.7	31	149
21-6-9/312M	1383	111.0	51	-
304L/312M	1058	71.3	25	119
21-6-9/308L	1532	123.0	57	68
304L/312M	770	51.9	18	86
304L/308L	1532	-	-	170
304L/308L	1532	-	-	189

**Table III.** Volume Percent Ferrite and Mechanical and Fracture Toughness Properties

Material Description	Ferrite %	Yield Strength MPa	Ultimate Strength MPa	J <sub>0</sub> Uncharged kJ/sq. m	J <sub>0</sub> Hydrogen-Charged kJ/sq. m	J <sub>0</sub> Tritium-Charged-&-Aged 6 Mos. kJ/sq. m	J <sub>0</sub> Tritium-Charged-&-Aged 30 Mos. kJ/sq. m
Type 304L	0	462	724	242	133	165	178
Type 21-6-9	0	855	1007	179	-	117	66
304L EB Weld Weldment	4	-	-	1051	388	-	359
21-6-9/308L Weldment	6	545	752	909	114	300	-
304L/308L Weldment	8	427	607	744	135	218	251
304L/308L/312M Weldment	10	455	586	595	-	262	227
304L/308L/309LM Weldment	13	455	641	683	-	206	214
21-6-9/312M Weldment	24	490	745	366	30	89	-
304L/312M Weldment	25	490	724	193	30	77	99
304L/309LM	33	572	745	125	12	9	48